Contents lists available at ScienceDirect

Journal of Molecular Structure

journal homepage: www.elsevier.com

Vibrational spectroscopic investigations and molecular docking studies of biologically active 2-[4-(4-phenylbutanamido)phenyl]-5-ethylsulphonyl-benzoxazole

K. Jalaja[a, b], Monirah A. Al-Alshaikh[c], Y. Sheena Mary[d], C. Yohannan Panicker[d, *], Ali A. El-Emam[e], Ozlem Temiz-Arpaci[f], C. Van Alsenoy[g]

[a] Department of Physics, IES College of Engineering, Chittilappilly, Thrissur, Kerala, India
[b] R and D, Bharathiar University, Coimbatore, Tamilnadu, India
[c] Department of Chemistry, College of Science, King Saud University, Riyadh, 11451, Saudi Arabia
[d] Department of Physics, Fatima Mata National College, Kollam, Kerala, India
[e] Department of Pharmaceutical Chemistry, College of Pharmacy, King Saud University, Riyadh, 11451, Saudi Arabia
[f] Department of Pharmaceutical Chemistry, Ankara University, TR-06100 Tandogan, Ankara, Turkey
[g] Department of Chemistry, University of Antwerp, Groenenborgerlaan 171, B-2020, Antwerp, Belgium

ARTICLE INFO

Article history:
Received 27 January 2016
Received in revised form 1 June 2017
Accepted 11 July 2017
Available online xxx

Keywords:
DFT
Benzoxazole
Ethylsulphonyl
Molecular docking

ABSTRACT

The optimized molecular structure, vibrational wavenumbers, corresponding vibrational assignments of 2-[4-(4-phenylbutanamido)phenyl]-5-ethylsulphonyl-benzoxazole have been investigated experimentally and theoretically using Gaussian09 software. The wavenumbers were assigned by potential energy distribution and the frontier molecular orbital analysis is used to determine the charge transfer within the molecule. The stability of the molecule arising from hyper-conjugative interaction and charge delocalization has been analyzed using NBO analysis. The MEP analysis shows that the negative electrostatic potential regions are mainly localized over the oxygen's of the carbonyl and sulfonyl groups and nitrogen atom of the benzoxazole ring and are possible sites for electrophilic attack and the positive regions are localized over the NH group as possible sites for nucleophilic attack. From the molecular docking study, the ligand binds at the active sites of the protein by weak non-covalent interactions most prominent of which are H-bonding, cation-π and sigma-π interactions.

1. Introduction

Benzoxazoles are an important class of organic compounds, revealing a wealth of interesting applications and as such, have attracted much interest in the research community and naturally occurring benzoxazoles [1] continue to offer tempting lead structures for medicinal chemists to design novel drug candidates, aiming to expand upon the considerable therapeutic uses [2,3]. Metal derivatives of benzoxazole and benzothiazole have attracted much attention due to their optical and luminescent properties [4]. Derivatives of benzoxazole mainly exhibit antimicrobial [5,6] and antiviral [7,8] activities. The benzoxazole derivatives have been also under investigation because of their potential applicability using a light emitting element in light emitting devices and an electronic device [9,10]. Carboxyamidotriazole is a non-cytotoxic anti-tumor drug and it inhibits tumor cell proliferation and induces cell apoptosis in vitro and has been undergoing clinical trials for treating a variety of cancers [11,12]. Zeyrek et al. [13] reported the experimental and theoretical characterization of 2-(4-bromobenzyl)-5-ethylsulphonyl-1,3-benzoxazole. In the present study, both experimental and molecular modeling are combined for studying the optimized molecular structural parameters, vibrational spectra, total dipole moment, first and second order hyperpolarizabilities and HOMO-LUMO energies for the title compound using DFT/M05/6-311 + G(d,p) (5D, 7 F). In the present work, inhibitory of tyrosinase active 2-[4-(4-phenylbutanamido)phenyl]-5-ethylsulphonyl-benzoxazole (compound **3**) is re-synthesized [14] and molecular docking studies is reported.

2. Experimental details

2.1. Materials and methods

The chemicals and solvents were purchased from Sigma-Aldrich Co. (Taufkirchen, Munich Germany) and Fisher Scientific (Pittsburgh, PA, USA) and were used without purification. Silica gel HF_{254} chromatoplates (0.3 mm) were used for TLC and the mobile phase was chloroform/methanol (10:0.5) for compound **3** (2-[4-(4-phenylbutanamido)phenyl]-5-ethylsulphonyl-benzoxazole). Melting point was recorded on a Stuart Scientific SMP 1 (Bibby Scientific Limited, Staffordshire, UK) instrument and uncorrected. NMR spectra were recorded on a Varian Mercury 400 MHz NMR spectrometer (Palo Alto, CA, USA) in $CDCl_3$ or dimethylsulfoxide (DMSO-d_6); tetramethylsilane (TMS) was used as an internal stan-

* Corresponding author.
Email address: cyphyp@rediffmail.com (C.Yohannan Panicker)

http://dx.doi.org/10.1016/j.molstruc.2017.07.023
0022-2860/

dard. The mass spectra were recorded on a Waters ZQ Micromass LC-MS spectrometer (Milford, MA, USA) using the ESI (+) method. Elemental analyse was performed on an LECO 932 CHNS (St. Joseph, MI, USA) instrument and was within ±0.4% of theoretical value.

2.2. General for the preparation of compound 3

5-Ethylsulphonyl-2-(p-amino-phenyl)benzoxazole (**1**) was synthesized by heating 0.01 mol 4-ethylsulphonyl-2-aminophenol. HCl with 0.01 mol p-amino-benzoic acid in 24 g polyphosphoric acid was stirred 3 h. At the end of the reaction period, the resiude was poured into ice-water, stirred and was neutralized with excess of 10% NaOH solution extracted with benzene. The benzene solution was dried over anhydrous sodium sulphate and evaporated under diminished pressure. The residue was boiled with 200 mg charcoal in ethanol and filtered and a crude product was obtained and recrystallized from ethanol-water mixture and compound 1 was dried *in vacuo*. Benzene butanoic acid (0.5 mmol) and thionyl chloride (1.5 ml) were refluxed in benzene (5 ml) at 80C for 3 h excess thionyl chloride was removed *in vacuo*. The benzenebutanoyl chloride **(2)** were dissolved in ether (10 ml) and this solution added during 1 h to a stirred, ice-cold mixture of 5-ethylsulphonyl-2-[p-amino-phenyl]benzoxazole (**1),** (0.5 mmol), sodium bicarbonate (0.5 mmol), diethyl ether (10 ml) and water (10 ml). The mixture was kept stirred overnight at room temperature and filtered. The precipitate was washed with water, 2 N HCl and water, respectively and finally with ether to give **3** (Scheme 1, supporting material) [14]. The product was recrystallized from ethanol-water as needles which are dried *in vacuo*. The chemical, physical and spectral data of the compound **3** is reported below:

2.2.1. Compound 3:

2-[4-(4-phenylbutanamido)phenyl]-5-ethylsulphonyl-benzoxazole

$C_{25}H_{24}N_2O_4S$, yield: 41.72%, Mp: 250–251C. ^{1}H NMR (400 MHz, *d*-DMSO, (δ ppm) J = Hz): 10.327 (s, 1H), 8.263–8.259 (d, 1H, $J_{4,6}$=1.6 Hz), 8.193–8.171 (d, 2H, $J_{2',3'}$=$J_{6',5'}$=8.8 Hz), 8.051–8.029 (d, 1H, $J_{7,6}$=8.8 Hz), 7.936–7.910 (dd, 1H, $J_{6,4}$=1,6 Hz, $J_{6,7}$=8.6 Hz), 7.882–7.861 (d, 2H, $J_{3',2'}$=$J_{5',6'}$=8.8 Hz), 3.413–3.350 (m, 2H), 7.323–7.195 (m, 5H), 2.668–2.630 (t, 2H), 2.419–2.382 (t, 2H), 1.946–1.909 (m, 2H), 1.128 (t, 3H) MS (70 eV) *m/z*: 449.8 (M^++H)

The FT-IR spectrum (Fig. 1) was recorded using KBr pellets on a DR/Jasco FT-IR 6300 spectrometer. The FT-Raman spectrum (Fig. 2) was obtained on a Bruker RFS100/S FT-Raman spectrometer (Nd:YAG laser, 1064 nm excitation).

2.3. Tyrosinase, AChE and BChE inhibitory activity

Inhibition of tyrosinase (EC 1.14.1.8.1, 30U, mushroom tyrosinase, Sigma) was determined using the modified dopachrome method with L-DOPA as substrate [15]. Assays were conducted in a 96-well microplate and an ELISA microplate reader (VersaMax Molecular Device, USA) was used to measure absorbance at 475 nm. Forty microliters of compounds dissolved in DMSO with 80 µl of phosphate buffer (pH 6.8), 40 µl of L-DOPA were put each in well. Each sample was accompanied by a blank that had all the components except for L-DOPA. Results were compared with a control consisting of 50% DMSO in place of sample. The percentage tyrosinase inhibition was calculated as follows:

% Inhibiton = $(Absorbance_{control}-Absorbance_{sample})/Absorbance_{control}$x100.

AChE and BChE inhibitory activities were measured by slightly modifying the spectrophotometric method developed by Elmann et al. [16]. Electric eel AChE (Type-VI—S, EC3.1.1.7, Sigma) and horse serum BChE (EC 3.1.1.8, Sigma) were used while acetythiocholine iodide and butyrylthiocholine chloride (Sigma, St. Louis, MO, USA) were employed as substrates of the reaction. 5,5′-Dithio-bis(2-nitrobenzoic)acid (DTNB, Sigma, St. Louis, MO, USA) was used for the measurement of the anticholinesterase activity. All reagent and conditions were same as described in Ref. [17]. Briefly in this method, 140 µl of sodium phosphate buffer (pH8.0), 20 µl of test solution and 20 µlAChE/BChE solution were added by multichannel automatic pipette (Gilson pipetman, France) in a 96 well microplate and incubated for 15 min at 25 °C**.** The reaction was initiated with the addition of 10 µl acetythiocholine iodide/butyrylthiocholine chloride. Hydrolysis of acetythiocholine iodide/butyrylthiocholine chloride was monitored by the formation of the yellow 5-thio-2-nitro-benzoate anion as a result of reaction of DTNB with thiocholines, catalyzed by enzymes at 412 nm utilizing a 96-well microplate reader (VersaMax molecular Devices, USA). The measurements and calculations were evaluated by using Softmax PRO 4.3.2.IS software. Percentage of inhibition of AChE/BChE was determined by comparison of rates of reaction of samples relative to blank sample (ethanol in phosphate buffer pH 8.0) using the Formula (E-S)/E × 100, where E is the activity of enzyme without test sample and S is the activity of enzyme with test sample. The experiments were done in triplicate. Galanthamine used as reference was purchased from Sigma (St. Louis, MO, USA) (Table 1).

3. Computational details

Calculations of the title compound were carried out with Gaussian09 software program [18] using M05/6-311 + G(d,p) (5D, 7 F) basis set to predict the molecular structure and vibrational wavenumbers. Minnesota Functionals are developed by Truhlar's group is based on approximated exchange-correlation energy functionals in density functional theory. These functionals are meta-GGA approximations, include terms that depend on the kinetic energy density, and are based on flexible functional forms. M05 belongs to the first family of Minnesota functionals are published in 2005 and it includes dispersion effects which are not included in the case of widely used B3LYP functional. Zhao and Truhlar [19] have also demonstrated better performance of M05 over B3LYP for main group thermochemistry. Additionally, study by Zhao et al. [20] further confirms the performance of M05 family of functional when it comes to the general purpose applications in thermochemistry, kinetics, and noncovalent interactions involving nonmetals and suggests this functional to be used. We also decided to use it since it is also recommended to be used for studies involving both metallic and nonmetallic elements. It is expected that upon using this functional a better description of the geometric structure and calculated properties will be obtained [21]. Density functional theory has been proven to be extremely useful in treating the electronic structure of organic molecules. The basis set 6-311 + G(d,p) (5D, 7 F), which is an effective level with reasonable cost to study fairly large organic molecules, was utilized. As the DFT hybrid functional tends to overestimate the wavenumbers of the fundamental modes, a scaling factor of 0.9613 has been uniformly applied to the calculated wavenumbers [22]. The assignments of the calculated wavenumbers are aided by the animation option of GAUSSVIEW program [23] and potential energy distribution by GAR2PED software package [24]. The theoretically optimized geometrical parameters (Fig. 3) are given in Table 2.

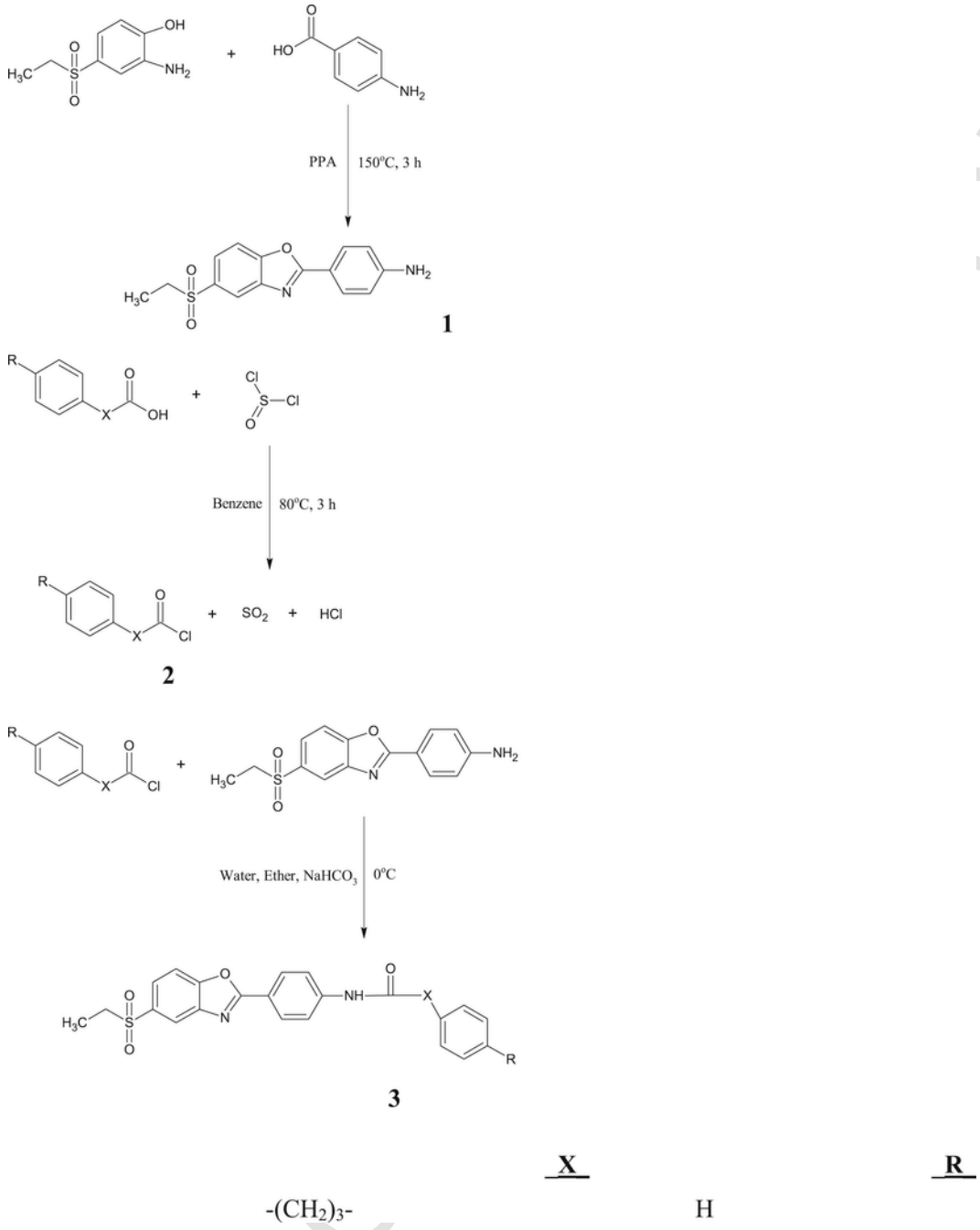

X	R
-(CH$_2$)$_3$-	H

Scheme 1. Synthesis of compound **3.**

4. Results and discussion

4.1. IR and Raman spectra

The calculated (scaled) wavenumbers, observed IR, Raman bands and assignments are given in Table 3. The NH stretching vibration [25] appears strongly and broadly in the region 3490 ± 60 cm^{-1}. For the title compound, the NH stretching band is observed in the IR spectrum at 3375 cm^{-1} and the theoretical value is 3524 cm^{-1}. The downshift of about 149 cm^{-1} in the IR spectrum is due to the strong intra-molecular hydrogen bonding [26]. The hyper-conjugative interactions, C_{21}—O_{23} from N_{22} of $n_1(N_{22})\rightarrow\pi^*(C_{21}—O_{23})$ and C_{21}—N_{22} from O_{23} of $n_2(O_{23})\rightarrow\sigma^*(C_{21}—N_{22})$ support the above argument. The CNH vibration in which N and H atoms move in opposite directions of carbon atom in the amide moiety appears at 1468 (IR), 1465 cm^{-1} (DFT) and the CNH vibration in which N and H atoms move in the same direction of carbon atom in the amide group appear at 1281 cm^{-1} (DFT) [27,28]. The NH rock in plane is assigned at 1218 cm^{-1} theoretically [26]. The out of plane wagging of NH [25] is active with a broad band in the region 790 ± 70 cm^{-1} and band at 834 cm^{-1} (DFT) is assigned as this mode. Panicker et al. [29] reported NH deformation bands at 1538, 1220 cm^{-1} in IR spectrum and at 1538, 1223 cm^{-1} theoretically. The NH deformation modes are reported at 1523, 1260, 1210, 875 cm^{-1} experimentally, 1518, 1256,

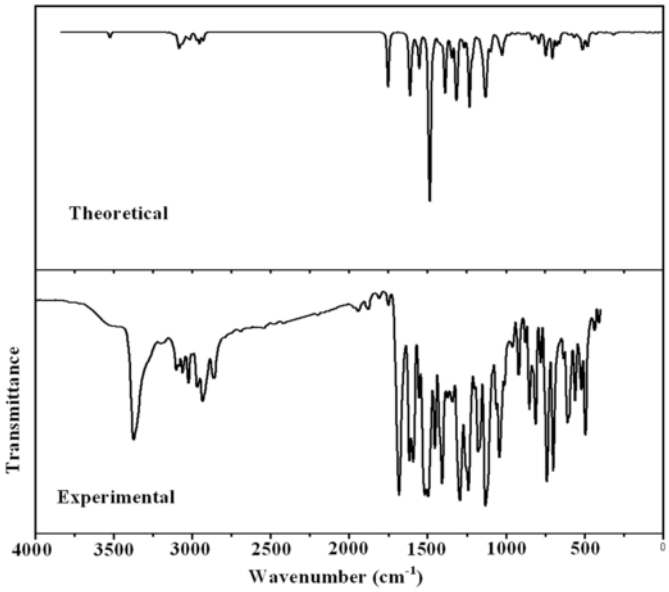

Fig. 1. FT-IR spectrum of 2-[4-(4-phenylbutanamido)phenyl]-5-ethylsulphonyl-benzoxazole.

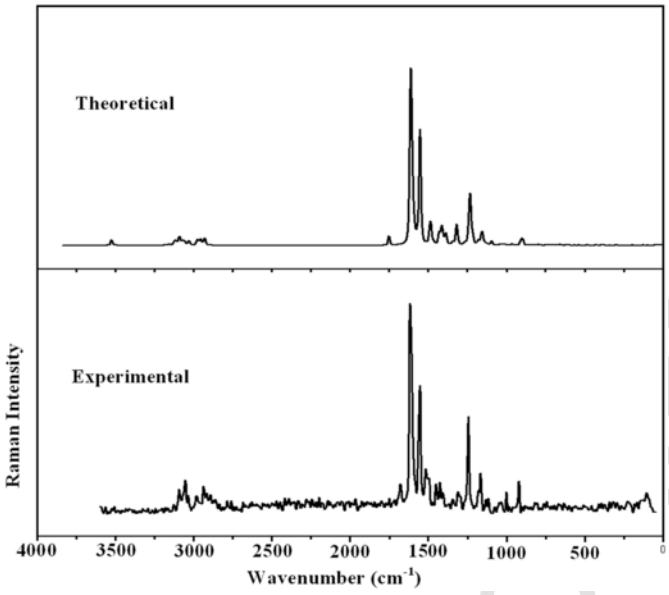

Fig. 2. FT-Raman spectrum of 2-[4-(4-phenylbutanamido)phenyl]-5-ethylsulphonyl-benzoxazole.

1221, 865 cm^{-1} theoretically by Sheeja et al. [26]. The CN stretching vibration [25] coupled with δNH is active in the region 1275 ± 55 cm^{-1}. In the present case the CN stretching band is observed at 1240 cm^{-1} in the IR spectrum and at 1237, 1229 cm^{-1} theoretically. Bhagyasree et al. [30] reported CN stretching modes at 1247 and 1236 cm^{-1} for a similar derivative. The C═N stretching mode is expected in the range 1670–1500 cm^{-1} [31,32] and in the present case this mode is assigned at 1617 cm^{-1} in the IR spectrum, 1616 cm^{-1} in the Raman spectrum and at 1614 cm^{-1} theoretically.

The carbonyl stretching C═O vibration [25,28,31] is expected in the region 1750-1680 cm^{-1} and in the present case this mode appears at 1751 cm^{-1} in IR spectrum, 1750 cm^{-1} in Raman spectrum. The DFT calculations give this mode at 1751 cm^{-1}. The in-plane and

Table 1
Tyrosinase, acetylcholinesterase (AChE) and butrylycholinesterase (BChE) inhibitory activity of the synthesized compound **3** [19].

Compound No	R	X	Inhibitory activity against tyrosinase (percentage ±SEM[a]) (2000 μg/ml	Inhibitory activity against AChE and BChE (percentage ±SEM) (2000 μg/ml)
3	−H	−(CH2)3−	54.29 ± 2.45	NA
Alpha-Kojic acid (reference for tyrosinase inhibition)			–	–
Galanthamine (reference for AChE, BChE inhibition)			–	

out-of-plane C═O deformations are expected in the regions 625 ± 70 and 540 ± 80 cm^{-1}, respectively [25]. The C═O deformation bands are observed at 561 cm^{-1} in the IR spectrum, 560 cm^{-1} in the Raman spectrum and at 651, 563 cm^{-1} theoretically. For the title compound, the COC stretching modes are observed at 1044 cm^{-1} in the IR spectrum, 1182 cm^{-1} in the Raman spectrum and at 1182, 1045 cm^{-1} theoretically as expected [30,31].

The asymmetric and symmetric stretching vibrations of SO_2 are reported in the range 1330 ± 60 and 1180 ± 45 cm^{-1} respectively [25]. For the title compound, the DFT calculations give these modes at 1313 and 1125 cm^{-1}. These SO_2 stretching modes are observed at 1130 cm^{-1} in the IR spectrum and at 1314, 1128 cm^{-1} in the Raman spectrum. The SO_2 deformation bands are expected in the regions 535 ± 40, 485 ± 50, 405 ± 65, 320 ± 40 cm^{-1} [25]. In the present case, these bands are observed at 511 cm^{-1} in the Raman spectrum and the DFT calculations give SO_2 modes at 513, 425, 379 and 327 cm^{-1} and most of the bands are not pure but contains significant contributions from other modes also. Rodriguez et al. [33] reported the SO_2 bands in the range 1242–1394, 590–632 and 460-470 cm^{-1}. The C—S stretching modes are assigned at 701 cm^{-1} in IR, 699 cm^{-1} in Raman and at 704, 660 cm^{-1} theoretically as expected [25].

The stretching vibrations of the CH_2 group (the asymmetric and symmetric stretch) appears in the regions 3000 ± 20 and 2900 ± 25 cm^{-1} respectively [25,28]. The CH_2 stretching modes are observed at 2970, 2932 cm^{-1} in the IR spectrum, 3030, 3010, 2980, 2934, 2920 cm^{-1} in the Raman spectrum and in the range 3032–2929 cm^{-1} theoretically. The deformation modes of CH_2 are observed at 1378, 1298, 1203 cm^{-1} in the IR spectrum, 1347, 1272, 1244, 1205 cm^{-1} in the Raman spectrum and in the range 1434–1100 cm^{-1} theoretically as expected [25]. The asymmetric stretching vibrations of CH_3 are expected in the range 2950–3050 cm^{-1} and symmetric CH_3 vibrations in the range of 2900–2950 cm^{-1} [25,28]. The stretching modes of the methyl group are calculated (DFT) to be 3050, 3027 and 2954 cm^{-1}. The bands observed at 3025 cm^{-1} in the IR spectrum and at 3030 cm^{-1} in the Raman spectrum was assigned as stretching modes of the methyl group. The deformation modes of the methyl group are assigned at 1430-952 cm^{-1} theoretically and only one band is observed in the IR spectrum at 1343 cm^{-1}. The methyl torsions [25] often assigned in the region 185 ± 65 cm^{-1}.

In the following discussion, the mono-, para- and tri-substituted phenyl rings and the benzoxazole ring are designated as PhI, PhII, PhIII and PhIV, respectively. The phenyl CH stretching modes are observed at 3082, 3064 (IR), 3093, 3056 (Raman) for PhI, 3105 (IR)

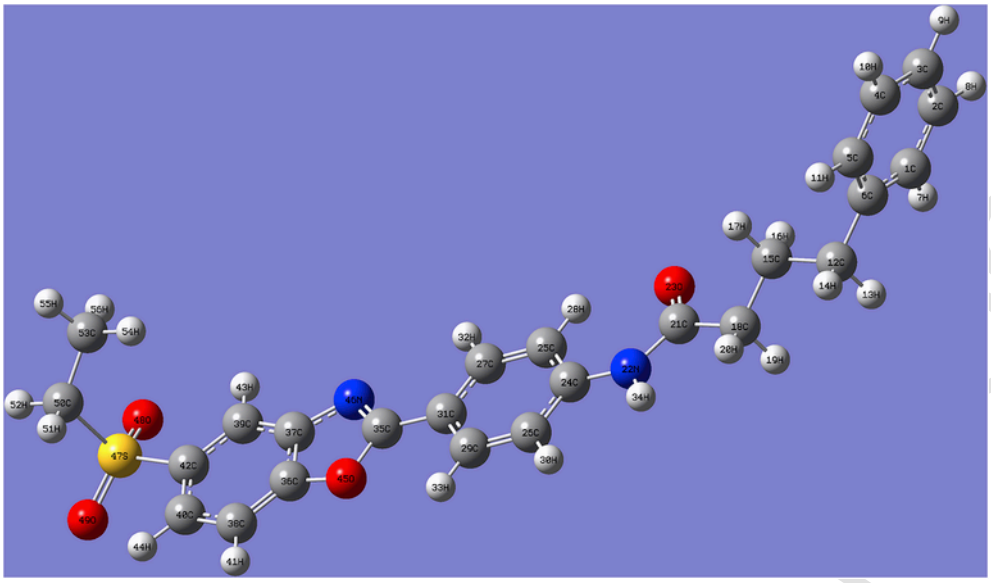

Fig. 3. Optimized geometry of 2-[4-(4-phenylbutanamido)phenyl]-5-ethylsulphonyl-benzoxazole.

for PhII and 3167 (IR), 3125 (Raman) for PhIII rings as expected [25]. The DFT calculations give these modes in the range 3091–3054 cm^{-1} for PhI, 3115-3071 cm^{-1} for PhII and 3157-3121 cm^{-1} for PhIII rings. The phenyl ring possesses six ring stretching modes and these modes are observed at 1458 (IR), 1458 (Raman) for PhI, 1490 (Raman) for PhII and 1593, 1555 (IR), 1554, 1427 cm^{-1} (Raman) for PhIII rings. These phenyl ring modes are expected in the range 1000–1600 cm^{-1} [25,27] and the DFT calculations give these modes in the range, 1602-1310 cm^{-1} for PhI, 1603-1320 cm^{-1} for PhII and 1591-1349 cm^{-1} for PhIII rings. The ring breathing mode of the phenyl ring appears as a weak band near 1000 cm^{-1} in mono substituted benzenes and in the present case the DFT calculations give 1010 cm^{-1} as the ring breathing mode for PhI. The ring breathing mode of the para substituted benzene compounds with entirely different substituents has been reported in the range 700–830 cm^{-1} and in the present case the band at 733 cm^{-1} (DFT) is assigned as the ring breathing mode of PhII [25]. In asymmetric tri-substituted benzene, when all the three substituents are light, the ring breathing mode falls in the range 500–600 cm^{-1}; when all the three substituents are heavy, it appears above 1100 cm^{-1} and in the case of mixed substituents, it falls in the range 600–750 cm^{-1} [27]. For the tri-substituted phenyl ring PhIII, the ring breathing mode is assigned at 1095 cm^{-1} theoretically. Madhavan et al. [34] reported the ring breathing mode for a compound having two tri-substituted benzene rings at 1110 and 1083 cm^{-1}. The in-plane and out-of-plane CH deformations of the phenyl rings are expected above 1000 cm^{-1} and below 1000 cm^{-1} [25]. In the present case, the in-plane CH deformation modes are observed at 1121, 1063 (IR), 1292, 1118, 1070 (Raman) for PhI, 1262, 1164 (IR), 1162, 982 (Raman) for PhII and at 1182 cm^{-1} (Raman) for PhIII rings. The out-of-plane CH deformations are assigned at 878 (IR), 820 (Raman) for PhI, 958, 923, 842, 788 cm^{-1} (IR), 958, 840, 789 (Raman) for PhII and at 920, 870 cm^{-1} (Raman) for PhIII. Most of the modes are not pure, but contains significant contributions from other modes also.

4.2. Geometrical parameters

The aromatic rings of the title compound are somewhat irregular and the spread of C—C bond distance is 1.3900–1.3961 in PhI, 1.3814–1.4012 in PhII and 1.3827–1.4022 Å for PhIII, which are similar to the spread reported by Bhagyasree et al. [35]. For the title compound, the CN bond lengths are, C_{35}—N_{46} = 1.2943, C_{37}—N_{46} = 1.3807, C_{24}—N_{22} = 1.3992 and C_{21}—N_{22} = 1.3829 Å. In the present case, the C═O bond length is 1.2104, C—O bond lengths are 1.3719, 1.3545 and S═O bond lengths are 1.4549 and 1.4550 Å. The C—O and C—N bond lengths are different because of the difference in electro-negativity between O, N and S atoms and also assume a double bond character in C_{35}—N_{46}. For the title compound, the C—S bond lengths are 1.8085 and 1.7923 Å. Mary et al. [36] reported the C—S and S═O bond lengths as 1.8021, 1.8260 Å and 1.4739, 1.4731 Å for a similar derivative. The bond angles at C_{35} position, C_{31}—C_{35}—O_{45} (117.2°), C_{31}—C_{35}—N_{46} (127.9°) and O_{45}—C_{35}—N_{46} (115.0°) indicates the π bond character of the bonds. Bond angles C_{39}—C_{37}—N_{46} (131.3°) and C_{38}—C_{36}—O_{45} (128.4°) are higher than 120° indicates the presence of hyper-conjugative interaction. At C_6 position, the bond angle C_1—C_6—C_5 is 118.2° and this reduction in angle from 120° reveals the interaction between the mono-substituted phenyl ring and the adjacent methylene groups. At C_{24} position, the bond angles, C_{25}—C_{24}—N_{22} is increased by 3.4° and C_{26}—C_{24}—N_{22} is reduced by 2.6° from 120°, which reveals the steric interaction between ring II and the NH group. Similarly at C_{21} position, the bond angles are N_{22}—C_{21}—O_{23} = 123.6, O_{23}—C_{21}—C_{18} = 122.6 and N_{22}—C_{21}—C_{18} = 113.8° and this asymmetry between the angles reveals the interaction between C═O group with the neighboring units. The changes in CCO and CCN angles are due to the difference in electronegativity between O, N and S atoms. The ethylsulphonyl moiety is tilted from the ring PhIII as is evident from the torsion angles C_{37}—C_{39}—C_{42}—S_{47} = 178.8, C_{39}—C_{42}—S_{47}—C_{50} = −95.0, C_{38}—C_{40}—C_{42}—S_{47} = −178.8 and C_{40}—C_{42}—S_{47}—C_{50} = 84.6°.

4.3. Frontier molecular orbitals

Knowledge of the highest occupied molecular orbital (HOMO) and lowest unoccupied molecular orbital (LUMO) and their properties such as their energy is very useful to gauge the chemical reactivity of the molecule. The HOMO and LUMO energies are very useful for physicists and chemists and are very important terms in

Table 2
Optimized geometrical parameters of the title compound.

Bond lengths (Å)					
C1—C2	1.3900	C1—C6	1.3961	C1—H7	1.0868
C2—C3	1.3905	C2—H8	1.0852	C3—C4	1.3903
C3—H9	1.0849	C4—C5	1.3903	C4—H10	1.0853
C5—C6	1.3960	C5—H11	1.0869	C6—C12	1.5045
C12—H13	1.0961	C12—H14	1.0960	C12—C15	1.5286
C15—H16	1.0926	C15—H17	1.0956	C15—C18	1.5215
C18—H19	1.0979	C18—H20	1.0955	C18—C21	1.5179
C21—N22	1.3829	C21—O23	1.2104	N22—C24	1.3992
N22—H34	1.0064	C24—C25	1.4006	C24—C26	1.4012
C25—C27	1.3838	C25—H28	1.0790	C26—C29	1.3814
C26—H30	1.0863	C27—C31	1.3976	C27—H32	1.0836
C29—C31	1.3981	C29—H33	1.0832	C31—C35	1.4528
C35—O45	1.3719	C35—N46	1.2943	C36—C37	1.3972
C36—C38	1.3827	C36—O45	1.3545	C37—C39	1.3917
C37—N46	1.3807	C38—C40	1.3889	C38—H41	1.0828
C39—C42	1.3894	C39—H43	1.0829	C40—C42	1.4022
C40—H44	1.0835	C42—S47	1.7923	S47—O48	1.4549
S47—O49	1.4550	S47—C50	1.8085	C50—H51	1.0918
C50—H52	1.0934	C50—C53	1.5130	C53—H54	1.0922
C53—H55	1.0925	C53—H56	1.0910		
Bond angles (°)					
C2—C1—C6	121.0	C2—C1—H7	119.5	C6—C1—H7	119.4
C1—C2—C3	120.1	C1—C2—H8	119.8	C3—C2—H8	120.1
C2—C3—C4	119.5	C2—C3—H9	120.3	C4—C3—H9	120.3
C3—C4—C5	120.1	C3—C4—H10	120.1	C5—C4—H10	119.8
C4—C5—C6	121.0	C4—C5—H11	119.5	C6—C5—H11	119.5
C1—C6—C5	118.2	C1—C6—C12	120.9	C5—C6—C12	120.9
C6—C12—H13	109.5	C6—C12—H14	109.3	C6—C12—C15	112.8
H13—C12—H14	106.4	H13—C12—C15	109.1	H14—C12—C15	109.5
C12—C15—H16	110.1	C12—C15—H17	109.4	C12—C15—C18	112.6
H16—C15—H17	106.1	H16—C15—C18	108.9	H17—C15—C18	109.5
C15—C18—H19	109.7	C15—C18—H20	110.5	C15—C18—C2	112.7
H19—C18—H20	106.3	H19—C18—C21	106.2	H20—C18—C21	111.0
C18—C21—N22	113.8	C18—C21—O23	122.6	N22—C21—O23	123.6
C21—N22—C24	129.5	C21—N22—H34	115.6	C24—N22—H34	114.8
N22—C24—C25	123.4	N22—C24—C26	117.4	C25—C24—C26	119.2
C24—C25—C27	119.6	C24—C25—H28	119.6	C27—C25—H28	120.8
C24—C26—C29	120.8	C24—C26—H30	119.8	C29—C26—H30	119.4
C25—C27—C31	121.4	C25—C27—H32	119.7	C31—C27—H32	118.9
C26—C29—C31	120.2	C26—C29—H33	119.7	C31—C29—H33	120.1
C27—C31—C29	118.8	C27—C31—C35	119.5	C29—C31—C35	121.7
C31—C35—O45	117.2	C31—C35—N46	127.9	O45—C35—N46	115.0
C37—C36—C38	124.2	C37—C36—O45	107.4	C38—C36—O45	128.4
C36—C37—C39	119.8	C36—C37—N46	108.9	C39—C37—N46	131.3
C36—C38—C40	115.8	C36—C38—H41	122.2	C40—C38—H41	122.0
C37—C39—C42	116.5	C37—C39—H43	122.0	C42—C39—H43	121.5
C38—C40—C42	120.7	C38—C40—H44	120.2	C42—C40—H44	119.1
C39—C42—C40	123.0	C39—C42—S47	118.7	C40—C42—S47	118.3
C35—O45—C36	104.4	C35—N46—C37	104.4	C42—S47—O48	107.9
C42—S47—O49	107.9	C42—S47—C50	104.5	O48—S47—O49	120.8
O48—S47—C50	107.9	O49—S47—C50	106.7	S47—C50—H51	105.7
S47—C50—H52	102.2	S47—C50—C53	114.6	H51—C50—H52	108.0
H51—C50—C53	113.3	H52—C50—C53	112.2	C50—C53—H54	111.8
C50—C53—H55	109.5	C50—C53—H56	110.9	H54—C53—H55	107.7
H54—C53—H56	108.6	H55—C53—H56	108.2		
Dihedral angles (°)					
C6—C1—C2—C3	−0.0	H7—C1—C2—C3	−179.9	H7—C1—C2—H8	−0.0
C2—C1—C6—C5	−0.0	C2—C1—C6—C12	178.2	H7—C1—C6—C5	179.8
H7—C1—C6—C12	−2.0	C1—C2—C3—C4	0.1	C1—C2—C3—H9	179.8
H8—C2—C3—C4	−179.7	H8—C2—C3—H9	0.0	C2—C3—C4—C5	−0.1
C2—C3—C4—H10	179.7	H9—C3—C4—C5	−179.8	H9—C3—C4—H10	−0.1
C3—C4—C5—C6	−0.0	C3—C4—C5—H11	179.6	H10—C4—C5—C6	−179.8
H10—C4—C5—H11	−0.1	C4—C5—C6—C1	0.1	C4—C5—C6—C12	−178.2
H11—C5—C6—C1	−179.6	H11—C5—C6—C12	2.1	C1—C6—C12—H13	34.0
C1—C6—C12—H14	150.2	C1—C6—C12—C15	−87.7	C5—C6—C12—H13	−147.8
C5—C6—C12—H14	−31.6	C5—C6—C12—C15	90.5	C6—C12—C15—H16	58.8
C6—C12—C15—H17	−57.4	C6—C12—C15—C18	−179.4	H13—C12—C15—H16	−63.1
H13—C12—C15—H17	−179.3	H13—C12—C15—C18	58.7	H14—C12—C15—H16	−179.1
H14—C12—C15—H17	64.7	H14—C12—C15—C18	−57.4	C12—C15—C18—H19	−56.6
C12—C15—C18—H20	60.3	C12—C15—C18—C21	−174.8	H16—C15—C18—H19	65.9
H16—C15—C18—H20	−177.2	H16—C15—C18—C21	−52.3	H17—C15—C18—H19	−178.6
H17—C15—C18—H20	−61.7	H17—C15—C18—C21	63.2	C15—C18—C21—N22	−146.0
C15—C18—C21—O23	35.4	H19—C18—C21—N22	93.8	H19—C18—C21—O23	−84.8
H20—C18—C21—N22	−21.4	H20—C18—C21—O23	160.0	C18—C21—N22—C24	−177.4
C18—C21—N22—H34	1.6	O23—C21—N22—C24	1.2	O23—C21—N22—H34	−180.0
C21—N22—C24—C25	−2.2	C21—N22—C24—C26	178.1	H34—N22—C24—C25	178.7
H34—N22—C24—C26	−0.9	N22—C24—C25—C27	−179.4	N22—C24—C25—H28	0.5
C26—C24—C25—C27	0.3	C26—C24—C25—H28	−179.8	N22—C24—C26—C29	179.5
N22—C24—C26—H30	−0.5	C25—C24—C26—C29	−0.2	C25—C24—C26—H30	179.8
C24—C25—C27—C31	−0.1	C24—C25—C27—H32	179.8	H28—C25—C27—C31	180.0
H28—C25—C27—H32	−0.1	C24—C26—C29—C31	−0.1	C24—C26—C29—H33	−180.0
H30—C26—C29—C31	179.9	H30—C26—C29—H33	0.0	C25—C27—C31—C29	−0.1
C25—C27—C31—C35	179.6	H32—C27—C31—C29	179.9	H32—C27—C31—C35	−0.3
C26—C29—C31—C27	0.2	C26—C29—C31—C35	−179.5	H33—C29—C31—C27	−179.9
H33—C29—C31—C35	0.4	C27—C31—C35—O45	179.3	C27—C31—C35—N46	−1.1
C29—C31—C35—O45	−1.0	C29—C31—C35—N46	178.7	C31—C35—O45—C36	179.6
N46—C35—O45—C36	−0.1	C31—C35—N46—C37	−179.6	O45—C35—N46—C37	0.1

C38—C36—C37—C39	0.4	C38—C36—C37—N46	−179.4	O45—C36—C37—C39	179.9
O45—C36—C37—N46	0.1	C37—C36—C38—C40	−0.5	C37—C36—C38—H41	178.7
O45—C36—C38—C40	−179.8	O45—C36—C38—H41	−0.6	C37—C36—O45—C35	−0.0
C38—C36—O45—C35	179.4	C36—C37—C39—C42	0.2	C36—C37—C39—H43	−178.5
N46—C37—C39—C42	180.0	N46—C37—C39—H43	1.2	C36—C37—N46—C35	−0.1
C39—C37—N46—C35	−179.9	C36—C38—C40—C42	−0.1	C36—C38—C40—H44	178.2
H41—C38—C40—C42	−179.3	H41—C38—C40—H44	−1.0	C37—C39—C42—C40	−0.8
C37—C39—C42—S47	178.8	H43—C39—C42—C40	178.0	H43—C39—C42—S47	−2.4
C38—C40—C42—C39	0.8	C38—C40—C42—S47	−178.8	H44—C40—C42—C39	−177.5
H44—C40—C42—S47	2.9	C39—C42—S47—O48	19.6	C39—C42—S47—O49	151.7
C39—C42—S47—C50	−95.0	C40—C42—S47—O48	−160.8	C40—C42—S47—O49	−28.7
C40—C42—S47—C50	84.6	C42—S47—C50—H51	−58.5	C42—S47—C50—H52	−171.4
C42—S47—C50—C53	67.0	O48—S47—C50—H51	−173.2	O48—S47—C50—H52	73.9
O48—S47—C50—C53	−47.7	O49—S47—C50—H51	55.7	O49—S47—C50—H52	−57.2
O49—S47—C50—C53	−178.8	S47—C50—C53—H54	−64.7	S47—C50—C53—H55	176.0
S47—C50—C53—H56	56.6	H51—C50—C53—H54	56.7	H51—C50—C53—H55	−62.6
H51—C50—C53—H56	178.0	H52—C50—C53—H54	179.3	H52—C50—C53—H55	60.1
H52—C50—C53—H56	−59.3				

quantum chemistry [37]. The pictorial representation of the HOMO and the LUMO is shown in Fig. 4. The HOMO lies at −8.30 eV and whereas the LUMO is located at −5.114 eV and is delocalized over the entire molecule with the exception, of the ethyl group of the ester function. This shows that an eventual charge transfer occurs within the molecule, and that the frontier orbital energy gap is 3.186 eV. The lower the energy gap the more easily are the electrons excited from the ground to the excited state. The energy gap explains the eventual charge transfer interaction within the molecule and is useful in determining molecular electrical transport properties. Both the HOMO and LUMO orbital are the main orbitals that decide on the chemical stability of the molecule. By using the HOMO and LUMO energy values, the global chemical reactivity descriptors such as hardness, chemical potential, electro-negativity and electrophilicity index as well as local reactivity can be defined [38]. Pauling introduced the concept of electro-negativity as the power of an atom in a molecule to attract electrons to it. Hardness (η), chemical potential (μ) and electro-negativity (χ) are defined using Koopman's theorem as $\eta = (I-A)/2 = 1.593$ eV, $\mu = -(I + A)/2 = -6.707$ eV and $\chi = (I + A)/2 = 6.707$ eV, where A and I are the ionization potential and electron affinity of the molecule. $I = -E_{HOMO} = 8.30$ eV and $A = -E_{LUMO} = 5.114$ eV. One can also relate the stability of the molecule to hardness, which means that the molecule with a lower energy gap shows higher reactivity. Parr et al. [39] have defined a descriptor to quantify the global electrophilic power of the molecule as the electrophilicity index, $\omega = \mu^2/2\eta = 14.192$ eV. The usefulness of this new reactivity quantity has been demonstrated recently in understanding the toxicity of various pollutants in terms of their reactivity and site selectivity [40].

Table 3
Calculated (scaled) wavenumbers, observed IR, Raman bands and assignments of the title compound.

M05/6-311 + G(d,p) (5D, 7F)					
$\upsilon(cm^{-1})$	IR_I	R_A	IR	Raman	Assignments[a]
-	-	-	$\upsilon(cm^{-1})$	$\upsilon(cm^{-1})$	-
3524	23.87	259.02	3375	–	υNH(100)
3157	3.41	67.97	3167	–	υCHIII(97)
3122	5.26	190.38	–	3125	υCHIII(99)
3121	1.28	23.09	–	–	υCHIII(93)
3115	5.13	63.32	–	–	υCHII(96)
3111	0.84	35.63	–	–	υCHII(97)
3108	1.30	43.13	3105	–	υCHII(99)
3091	20.27	331.72	–	3093	υCHI(96)
3083	48.91	61.42	3082	–	υCHI(95)
3071	28.21	105.84	–	–	υCHII(95)
3065	22.98	89.13	3064	–	υCHI(96)
3057	9.15	84.26	–	–	υCHI(94)
3054	7.43	30.47	–	3056	υCHI(100)
3050	15.60	11.89	–	–	υCH_3(69), υCH_2(29)
3032	8.59	117.22	–	3030	υCH_3(33), υCH_2(66)
3027	15.56	88.19	3025	3030	υCH_3(73), υCH_2(26)
3014	25.89	6.02	–	3010	υCH_2(86)
2976	4.43	209.80	–	2980	υCH_2(98)
2975	8.04	27.68	–	–	υCH_2(88)
2972	20.74	65.54	2970	–	υCH_2(96)
2954	18.17	187.19	–	–	υCH_3(100)
2951	29.51	22.97	–	–	υCH_2(94)
2931	40.36	321.09	2932	2934	υCH_2(98)
2929	2.12	30.61	–	2920	υCH_2(100)
1751	216.57	254.83	1751	1750	υC = O(78)
1614	213.17	3996.78	1617	1616	υC = N(45),υPhIII(10), υPhII(20)
1603	66.47	1986.46	–	–	υPhII(51), υPhIII(10)
1602	25.57	86.00	–	–	υPhI(60), υPhIII(15)
1591	13.71	450.15	1593	–	υPhIII(61), υPhI(13)
1576	0.82	9.30	–	–	υPhI(72), υPhII(11)
1570	32.08	183.99	–	–	υPhII(53), υPhIII(14)
1552	129.58	2959.63	1555	1554	υC = N(24), υPhII(16), υPhIII(41)
1487	1042.44	943.16	–	1490	δNH(14), υCN(17), δCHII(10), υPhII(44)
1465	19.95	62.38	1468	–	δNH(40), δCHII(28), υPhII(20)
1461	18.53	2.06	1458	1458	δCHI(22), υPhI(48)
1434	12.12	1.85	–	–	δCH_2(89)
1430	3.71	135.96	–	–	δCH_3(47), υPhIII(16), δCHIII(12)
1429	13.40	203.61	–	1427	δCH_3(39), υPhIII(45)
1423	7.17	19.89	–	–	δCH_3(94)
1418	3.08	18.28	–	–	δCH_2(25), δCHI(12), υPhI(47)
1417	2.39	18.77	–	–	δCH_2(52), δCHI(10), υPhI(13)
1411	38.19	613.06	1408	1408	υPhIII(43), υCN(18), δCHIII(15)
1397	25.35	12.64	–	–	δCH_2(87)
1386	245.12	310.73	–	–	υPhII(48), δCHII(28)
1380	9.01	8.69	1378	–	δCH_2(90)
1349	64.83	18.40	–	–	δCH_3(20), υPhIII(41)
1347	44.23	59.29	–	1347	δCH_2(54), υCC(25)
1342	14.42	13.16	1343	–	δCH_3(50), υPhIII(44)
1320	173.51	524.07	–	–	υPhII(56), δCH_2(14)
1313	177.23	25.15	–	1314	υSO_2(75)
1310	8.64	14.84	–	–	υPhI(74)
1308	11.85	35.04	1298	–	δCH_2(52), δCHI(22)
1288	0.21	0.66	–	1292	δCHI(79), δCH_2(13)
1281	17.06	4.29	–	–	δNH(41), υCC(12), υPhII(16), υCO(13)
1270	4.27	12.10	–	1272	δCH_2(64)
1267	43.18	36.83	1262	–	δCHII(69)
1246	24.27	35.88	–	1244	δCH_2(70), υSO_2(12)
1237	37.52	635.56	1240	–	υCN(44), δCH_2(25)

Table 3 (*Continued*)

M05/6-311 + G(d,p) (5D, 7F)					
$\upsilon(cm^{-1})$	IR_I	R_A	IR	Raman	Assignments[a]
-	-	-	$\upsilon(cm^{-1})$	$\upsilon(cm^{-1})$	-
1233	233.71	726.87	–	–	δCH_2(56), υCN(21)
1229	37.52	287.18	–	–	υCN(48), δCH_2(29)
1218	14.06	187.99	–	–	δCHIII(45), δNH(39)
1214	59.30	56.86	–	–	δCH_2(62), δCH_3(15)
1206	18.70	4.25	1203	1205	δCH_2(66), δCH_3(19)
1183	4.07	48.58	1180	–	υCC(28), δCH_2(19)
1182	11.28	63.32	–	1182	υCO(41), δCHIII(45)
1158	67.31	499.34	1164	1162	δCHII(75)
1147	0.60	3.96	–	–	δCHI(81), υPhI(11)
1140	215.20	53.14	–	–	υCN(29), δCH_2(24)
1125	280.27	40.95	1130	1128	υSO_2(81)
1121	1.20	4.62	1121	1118	δCHI(81), υPhI(12)
1100	68.30	35.15	–	–	δCH_2(56), δCHIII(17), υPhIII(12)
1095	8.40	22.01	–	–	δCHIII(51), υPhIII(44)
1094	16.14	59.01	–	–	υPhII(18), δCHII(53)
1060	7.43	2.82	1063	1070	υPhI(24), δCHI(49)
1046	4.01	2.25	–	–	υCC(45), δCH_3(25)
1045	29.15	6.78	1044	–	υCC(27), υCO(40)
1041	10.40	23.58	–	–	υCC(49), υPhIII(13), δCHIII(10)
1028	92.07	2.08	–	1031	υPhIII(44), δCHIII(22), υCO(12)
1022	31.09	33.87	–	–	υCC(63), δCH_2(13)
1012	9.67	3.97	–	–	δCH_3(46), δCH_2(48)
1010	4.39	21.03	–	–	δCHI(39), υPhI(56)
1005	12.55	0.79	1007	1002	δCH_2(65), δCHII(10), υPhI(11)
980	12.77	3.86	–	982	δCHII(50), υPhI(16)
966	0.53	38.55	–	–	δPhI(16), γCHI(76)
958	0.35	0.41	958	958	γCHII(96)
953	0.01	0.05	–	–	γCHI(80), τPhI(12)
952	2.23	2.64	–	–	δCH_3(44), υCC(28), δCH2(15)
941	10.96	2.45	–	–	υCC(33), δNH(14), υCN(22)
937	0.01	0.04	–	–	γCHI(92)
921	0.43	0.43	923	–	γCHII(87)
919	0.02	0.94	–	920	γCHIII(79), τPhII(13)
907	7.57	183.58	–	904	δPhIV(47), υCO(23), υPhIII(10)
895	5.40	99.85	–	892	δPhIII(47), γCHI(23)
881	1.09	1.06	878	–	γCHI(80), τPhI(12)
876	7.84	1.70	–	870	γCHIII(79), τPhIII(10)
836	19.14	1.33	842	840	γCHII(62)
834	9.30	1.00	–	–	γNH(44), γCHII(18)
819	1.59	0.91	–	820	γCHI(77)
815	7.49	3.91	813	–	δCH_2(26), γCHI(26)
807	8.40	4.39	–	805	υCC(20), δCH_2(22), δPhI(18), δPhII(15)
796	1.46	26.01	–	–	υCC(19), γCHIII(20), δPhI(22), δPhII(25)
793	2.44	3.96	–	–	γCHII(27), γCHIII(30)
791	37.41	0.62	788	789	γCHII(48), γCHIII(30)
749	82.91	3.71	–	–	δCH_2(53), δCH_3(22)
741	18.14	8.63	742	742	τPhI(25), γCHI(14), γCC(11), *dC* = O(11)
736	0.85	1.94	–	–	τPhIII(49), τPhIV(27)
733	21.53	5.63	–	–	υPhII(45), γCC(20), τPhIV(15), τPhIII(11)
723	5.36	4.78	–	725	τPhI(32), γCHI(19), δCH_2(20)
709	3.95	9.91	–	712	δCH_2(77)
704	93.47	10.35	701	699	υCS(47), δSO_2(12), δPhIV(12)
689	6.14	1.84	–	–	τPhII(51), τPhIV(14), γCN(10)
680	46.65	0.40	–	668	τPhI(54), γCHI(36)
660	41.55	16.77	–	–	δPhIV(21), υCS(38), δPhIII(15)
651	0.66	10.29	–	–	δPhII(29), γC = O(20), δPhIV(24)
616	1.61	8.73	–	618	δPhII(77)
605	0.04	4.32	606	–	δPhI(87)

Table 3 (*Continued*)

M05/6-311 + G(d,p) (5D, 7F)					
$\upsilon(cm^{-1})$	IR_I	R_A	IR	Raman	Assignments[a]
-	-	-	$\upsilon(cm^{-1})$	$\upsilon(cm^{-1})$	-
598	3.65	5.52	–	600	γCS(23), τPhIII(42)
596	14.00	0.86	596	–	γC = O(25), δPhI(20), δPhIII(24)
568	11.81	3.20	–	572	δPhIV(21), δPhI(20), δPhII(22), δPhIII(19)
563	17.26	1.55	561	560	δPhI(32), *dC* = O(40), δCH_2(10)
537	12.34	2.72	–	–	δPhIII(29), δCC(23), γNH(12)
527	18.71	2.17	525	530	γNH(31), γC = O(20)
513	63.15	0.98	–	511	δSO_2(62), δPhIII(10)
503	27.20	0.39	–	–	τPhII(36), γCN(26), γCC(20)
488	19.25	2.40	490	–	τPhI(50), γCC(24)
479	44.92	2.37	–	–	δSO_2(38), δCH2(13), τPhIII(15)
428	3.75	2.61	430	–	τPhIV(24), τPhIII(39)
425	4.75	3.71	–	–	τPhIV(18), τPhIII(16), δSO2(45)
396	0.00	0.05	–	–	τPhII(80)
394	0.43	3.79	–	394	δCN(27), τPhI(22), δCC(20)
393	0.02	0.14	–	394	τPhI(82)
379	0.74	2.27	–	–	τPhIII(27), τPhII(10), δSO_2(43)
376	2.93	1.74	–	375	δCN(28), δCC(10), δSO2(10)
345	4.18	2.40	–	344	δSO_2(22), δCN(10), δCC(10), δNH(10)
341	0.83	0.62	–	–	δCC(62), τCH_2(10)
327	1.29	2.02	–	–	δSO_2(36), γCS(10), γCC(10), τPhIII(10)
317	13.04	0.25	–	319	τPhI(29), δCH2(24)
298	3.42	6.55	–	296	δCH_2(24), δPhII(22), δCS(22)
280	1.72	0.93	–	–	δSO_2(22), δCC(19), τPhI(15), δCN(20)
262	0.46	1.00	–	264	τPhII918), τPhIV(11),γCC(15), τPhIII(10)
250	1.77	0.86	–	–	τPhIII(29), τCH_3(19), δSO_2(10), γCS(10)
222	0.86	0.98	–	225	δCS(25), δCH_2(18), δPhIII(20)
206	1.02	0.49	–	–	τCH_3(40), δCH_2(21), δSO_2(21)
195	2.49	3.31	–	–	τPhI(29), δCH_2(26)
193	2.19	0.76	–	–	δSO_2(19), τPhIII(20), τPhI(12), δCH_2(11)
163	2.03	1.37	–	165	δSO_2(18), τC = O(14), γNH(17), τPhII(20)
146	1.63	1.07	–	143	δCS(29), δSO_2(11), δPhII(12)
126	0.81	2.94	–	–	δPhII(23), δCH_2(20), δNH(18)
120	1.31	1.12	–	–	τCH_2(26), δNH(15), γCS(18)
101	0.33	1.71	–	104	τCH_2(74)
98	3.44	0.55	–	–	τCH_2(38), γCS(21)
81	0.43	0.73	–	–	τCH_2(32), δCH_2(20)
66	2.88	0.61	–	–	τNH(32), τCH_2(25)
59	1.67	0.73	–	–	τCC(26), τNH(25), τSO_2(13)
55	0.25	0.96	–	–	δCH_2(36), τCC(26)
43	0.41	1.47	–	–	τSO_2(19), τCC(14), τNH(13), δCC(14)
39	1.20	0.98	–	–	τSO_2(44), τCC(11)
30	0.95	6.16	–	–	τCC(36), τSO_2(10)
25	1.74	0.27	–	–	τCC(24), τCH_2(25), τNH(18)
19	0.08	6.72	–	–	τCC(30), τCH_2(34)
17	0.37	3.37	–	–	τCH_2(34), τSO_2(10)
6	0.91	3.02	–	–	τC = O(24), τPhII(15), τCC(18)

[a] υ-streching; δ-in-plane deformation; γ -out-of-plane deformation; τ-torsion; potential energy distribution (%) is given in the brackets in the assignment column; mono-, para- and tri-substituted phenyl rings and the benzoxazole ring are designated as PhI, PhII, PhIII and PhIV.

4.4. Nonlinear optical studies

Nonlinear optics deals with the interaction of applied electromagnetic fields in various materials to generate new electromagnetic

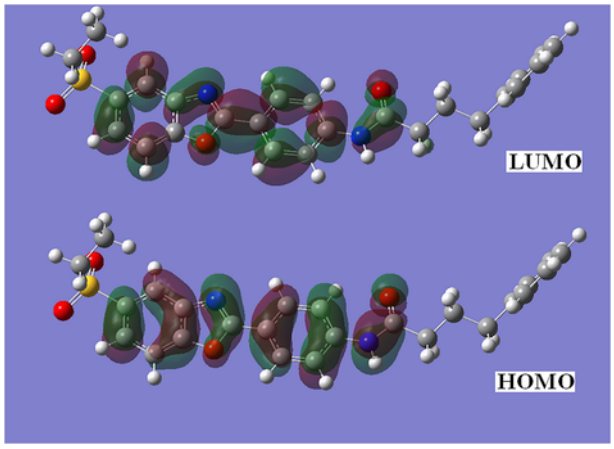

Fig. 4. HOMO-LUMO plots of 2-[4-(4-phenylbutanamido)phenyl]-5-ethylsulphonyl-benzoxazole.

fields, altered in wavenumber, phase, or other physical properties [41]. Quantum chemical calculations have been shown to be useful in the description of the relationship between the electronic structure of systems and its NLO response [42]. The first order hyperpolarizability of the title compound is calculated (using M05/6-311 + G(d,p) (5D, 7 F) basis set) and is found to be 14.7×10^{-30} esu. The calculated hyperpolarizability of the title compound is 113.08 times that of the standard NLO material urea (0.13×10^{-30} esu) [43]. The theoretical second order hyperpolarizability was calculated using the Gaussian09 software and is equal to -97.5×10^{-37} esu. We conclude that the title compound and its derivatives are an attractive object for future studies of nonlinear optical properties.

4.5. Molecular electrostatic potential

Molecular electrostatic potential (MEP) at a point in space around a molecule gives information about the net electrostatic effect produced at that point by the total charge distribution over the molecule [44]. Moreover, the MEP surface helps to predict the reactivity of a wide variety of chemical systems in both electrophilic and nucleophilic reactions, the study of biological recognition processes and hydrogen bonding interactions [45]. The different values of the electrostatic potential at the surface are represented by different colors; red represents regions of most electro negative electrostatic potential, blue represents regions of most positive electrostatic potential and green represents regions of zero potential. The electrostatic potential increases in the order red < orange < yellow < green < blue [44]. To predict reactive sites for electrophilic and nucleophilic attack in the investigated molecule, the MEP surface is plotted for the title compound at DFT level [46]. Fig. 5 shows the electrostatic potential contour map of the title compound. The negative electrostatic potential corresponds to an attraction of a proton by the aggregate electron density in the molecule (shades of red and yellow) and the positive electrostatic potential corresponds to the repulsion of a proton by the nuclei (shades of blue). As can be seen from Fig. 5, the negative electrostatic potential regions are mainly localized over the oxygen's of the carbonyl and sulfonyl groups and nitrogen atom of the benzoxazole ring and are possible sites for electrophilic attack. The positive regions are localized over the NH group as possible sites for nucleophilic attack.

4.6. Natural bond orbital analysis

The natural bond orbital (NBO) calculations were performed using NBO 3.1 program [47] as implemented in the Gaussian09 package at the M05/6-311 + G(d,p) (5D, 7 F) and in NBO analysis large stabilization energy E(2) value shows the intensive interaction between electron donors and electron-acceptors and the possible intensive interaction are given in Table 4. The various important hyper-conjugative interactions are: C_{21}—O_{23} from N_{22} of $n_1(N_{22}) \rightarrow \pi^*(C_{21}—O_{23})$, C_{21}—N_{22} from O_{23} of $n_2(O_{23}) \rightarrow \sigma^*(C_{21}—N_{22})$, C_{35}—N_{46} from O_{45} of $n_2(O_{45}) \rightarrow \pi^*(C_{35}—N_{46})$, S_{47}—O_{49} from O_{48} of $n_3(O_{48}) \rightarrow \pi^*(S_{47}—O_{49})$, S_{47}—O_{48} from O_{49} of $n_3(O_{49}) \rightarrow \pi^*(S_{47}—O_{48})$ with electron densities, 0.25556, 0.08093, 0.31126, 0.14398, 0.14511 e and stabilization energies, 54.56, 28.40, 34.74, 23.21, 23.38 kJ/mol. The NBO analysis also describes the bonding in terms of the natural hybrid orbital lone pair atoms and the orbitals with higher energy and considerable p-character (100%) are: $n_2(O_{23})$, $n_2(O_{45})$, $n_3(O_{48})$, $n_3(O_{49})$ with higher energy orbitals, −0.25593, −0.35152, −0.27384, −0.27331 a.u and low occupation numbers, 1.85982, 1.72496, 1.78711, 1.78655. The orbitals with lower energy and high occupation numbers are: $n_1(O_{23})$, $n_1(O_{45})$, $n_1(O_{48})$, $n_1(O_{49})$ with lower energy orbitals, −0.67797, −0.59820, −0.76111, −0.76120 a.u and p-characters, 42.81, 63.36, 26.67, 26.58% and high occupation numbers, 1.97414, 1.96833, 1.98228, 1.98218. Thus, a very close to pure p-type lone pair orbital participates in the electron donation to the π^*(C—C) orbitals for $n_2(O_{45}) \rightarrow \pi^*$(C—C) and $n_2(O_{23}) \rightarrow \pi^*$(C—C) interactions respectively in the compound. The results are tabulated in Table 5.

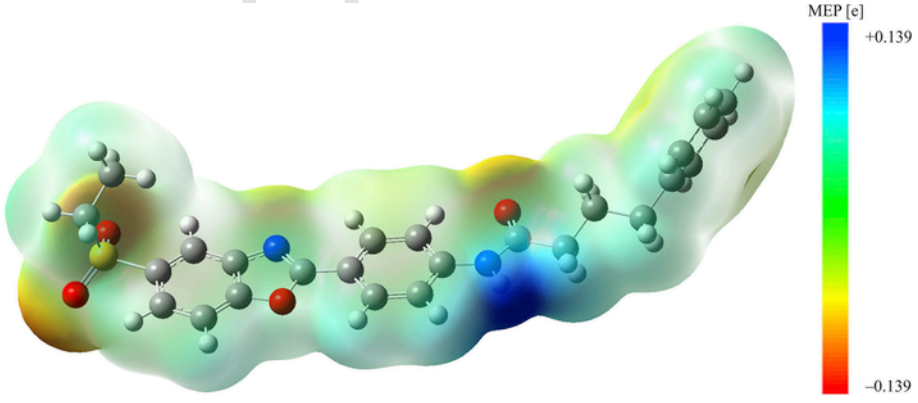

Fig. 5. MEP plot of 2-[4-(4-phenylbutanamido)phenyl]-5-ethylsulphonyl-benzoxazole.

Table 4
Second-order perturbation theory analysis of Fock matrix in NBO basis corresponding to the intramolecular bonds of the title compound.

Donor(i)	type	ED/e	Acceptor(j)	Type	ED/e	E(2)[a]	E(j)-E(i)[b]	F(i,j)[c]
C1—C2	π	1.67037	C3—C4	π*	0.33509	19.96	0.28	0.067
–	π	–	C5—C6	π*	0.33509	21.23	0.29	0.070
C3—C4	π	1.66463	C1—C2	π*	0.33045	20.94	0.28	0.069
–	π	–	C5—C6	π*	0.33509	19.77	0.29	0.067
C5—C6	π	1.97469	C1—C2	π*	0.33045	19.75	0.28	0.067
–	π	–	C3—C4	π*	0.33509	21.50	0.28	0.070
C24—C26	π	1.62827	C25—C27	π*	0.28335	15.56	0.30	0.063
–	π	–	C29—C31	π*	0.40936	23.78	0.29	0.075
C25—C27	π	1.67279	C24—C26	π*	0.40501	23.41	0.27	0.072
–	π	–	C29—C31	π*	0.40936	17.92	0.28	0.064
C29—C31	π	1.63270	C24—C26	π*	0.40501	18.64	0.27	0.064
–	π	–	C25—C27	π*	0.28335	20.66	0.29	0.071
–	π	–	C35—N46	π*	0.28335	24.14	0.26	0.072
C35—N46	π	1.85814	C37—C39	π*	0.39515	20.77	0.35	0.082
C36—C38	π	1.64007	C37—C39	π*	0.39515	18.04	0.30	0.066
–	π	–	C40—C42	π*	0.42799	23.19	0.28	0.074
C37—C39	π	1.59523	C36—C38	π*	0.39718	23.82	0.28	0.073
–	π	-C40-C42	π*	0.42799	20.04	0.27	0.066
C40—C42	π	1.67545	C37—C39	π*	0.39515	20.68	0.29	0.071
LPN22	σ	1.66510	C21—O23	π*	0.25556	54.56	0.29	0.115
–	σ	–	C24—C26	π*	0.40501	35.34	0.29	0.092
LPO23	π	1.85982	C18—C21	σ*	0.06178	20.78	0.64	0.105
–	π	–	C21—N22	σ*	0.08093	28.40	0.69	0.127
LPO45	π	1.72496	C35—N46	π*	0.31126	34.74	0.36	0.100
–	π	–	C36—C38	π*	0.39718	29.79	0.37	0.096
LPN46	σ	1.90961	C35—O45	σ*	0.06256	14.48	0.70	0.090
LPO48	π	1.82053	C42—S47	σ*	0.20749	13.89	0.45	0.071
–	π	–	S47—C50	σ*	0.19913	16.39	0.42	0.075
LPO48	n	1.78711	S47—O49	σ*	0.14398	23.21	0.58	0.106
LPO49	π	1.82226	C42—S47	σ*	0.20749	14.03	0.45	0.071
–	π	–	S47—C50	σ*	0.19913	15.61	0.42	0.073
LPO49	n	1.78655	S47—O48	σ*	0.14511	23.38	0.58	0.106

[a] E(2) means energy of hyper-conjugative interactions (stabilization energy in kJ/mol).
[b] Energy difference (a.u.) between donor and acceptor i and j NBO orbitals.
[c] F(i,j) is the Fock matrix elements (a.u.) between i and j NBO orbitals.

Table 5
NBO results showing the formation of Lewis and non-Lewis orbitals.

Bond (A–B)	ED/e[a]	EDA%	EDB %	NBO	s%	p%
σC1-C2	1.97936	50.22	49.78	0.7087(sp1.81)C	35.53	64.43
–	−0.68668	–	–	+0.7056(sp1.83)C	35.29	64.67
πC1-C2	1.67037	50.49	49.51	0.7105(sp1.00)C	0.00	100.0
–	−0.24125	–	–	+0.7037(sp1.00)C	0.00	100.0
σC3-C4	1.98019	49.93	50.07	0.7066(sp1.84)C	35.17	64.79
–	−0.68656	–	–	+0.7076(sp1.83)C	35.27	64.67
πC3-C4	1.66463	50.35	49.65	0.7096(sp1.00)C	0.00	100.0
–	−0.24089	–	–	+0.7046(sp1.00)C	0.00	100.0
σC5-C6	1.97469	49.25	50.75	0.7018(sp1.82)C	35.46	64.50
–	−0.68460	–	–	+0.7124(sp1.93)C	34.13	65.83
πC5-C6	1.65365	50.74	49.26	0.7123(sp1.00)C	0.00	100.0
–	−0.23909	–	–	+0.7019(sp1.00)C	0.00	100.0
σC24-C26	1.97489	51.02	48.98	0.7143(sp1.82)C	35.45	64.51
–	−0.71221	–	–	+0.6999(sp1.90)C	34.47	65.49
πC24-C26	1.62827	47.11	52.89	0.6864(sp1.00)C	0.00	100.0
–	−0.26601	–	–	+0.7273(sp1.00)C	0.00	100.0
σC25-C27	1.97635	50.03	49.97	0.7073(sp1.81)C	35.54	64.42
–	−0.70300	–	–	+0.7069(sp1.79)C	35.80	64.16
πC25-C27	1.67279	52.31	47.69	0.7233(sp1.00)C	0.00	100.0
–	−0.25435	–	–	+0.6906(sp1.00)C	0.00	100.0
σC29-C31	1.97319	48.62	51.38	0.6973(sp1.89)C	34.54	65.42
–	−0.70348	–	–	+0.7168(sp1.90)C	34.47	65.50
πC29-C31	1.63270	45.88	54.12	0.6774(sp1.00)C	0.00	100.0
–	−0.25813	–	–	+0.7357(sp1.00)C	0.00	100.0
σC35-N46	1.98509	41.20	58.80	0.6419(sp1.79)C	35.81	64.15
–	−0.87932	–	–	+0.7668(sp1.74)C	36.45	63.31
πC35-N46	1.85814	40.18	59.82	0.6339(sp1.00)C	0.00	100.0
–	−0.33011	–	–	+0.7734(sp1.00)N	0.00	100.0
σC40-C42	1.97712	48.93	51.07	0.6995(sp1.91)C	34.40	65.56
–	−0.72108	–	–	+0.71469sp1.66)C	37.62	62.34
πC40-C42	1.67545	44.49	55.51	0.66709sp1.00)C	0.00	100.0
–	−0.27172	–	–	+0.7451(sp1.00)C	0.00	100.0
n1O23	1.97414	–	–	sp0.75	57.13	42.81
–	−0.67797	–	–	–	–	–
n2O23	1.85982	–	–	sp1.00	0.00	100.0
–	−0.25593	–	–	–	–	–
n1O45	1.96833	–	–	sp1.73	36.58	63.36
–	−0.59820	–	–	–	–	–
n2O45	1.72496	–	–	sp1.00	0.00	100.0
–	0.35152	–	–	–	–	–
n1O48	1.98228	–	–	sp0.36	73.31	26.67
–	−0.76111	–	–	–	–	–
n2O48	1.82053	–	–	sp1.00	0.00	100.0
–	−0.27571	–	–	–	–	–
n3O48	1.78711	–	–	sp1.00	0.00	100.0
–	−0.27384	–	–	–	–	–
n1O49	1.98218	–	–	sp0.36	73.39	26.58
–	−0.76120	–	–	–	–	–
n2O49	1.82226	–	–	sp1.00	0.00	100.0
–	−0.27502	–	–	–	–	–
n3O49	1.78655	–	–	sp1.00	0.00	100.0
-	−0.27331	-	-	-	-	-

[a] ED/e is expressed in a.u.

4.7. Biological activity and molecular docking

In this work we have used several freely available online tools in order to calculate important descriptors valuable for the assessment of potential biological activity. Firstly, using ALGOPS 2.1 program [48], we have calculated values of well known parameters, logP and logS, frequently used for the assessment of important pharmaceutical properties. LogP denotes octanol/water partition coefficient and this parameter is usually employed for the assessment of lipophilicity of molecules. If logP takes value of ≤2 then such molecule is a candidate for the transdermal delivery [49], while according to Yano et al. [50] the optimal value of logP for nonsteroidal anti-inflammatory drugs is ∼2.5. The calculated logP value for the title molecule is rather high (4.4) for transdermal use, but it is relatively close to the logP values of commercially known drug such as indomethacin (3.8) [51]. Another important parameter for the drug delivery is aqueous solubility (logs), which is also readily available for calculation with

ALGOPS 2.1 program. Calculated value of logS in the case of title molecule is −4.83. Although more than 80% of drug molecules have logs values higher than −4.0, there are also many molecules with logs between −4.0 and −6.0 [52], emphasizing relatively good aqueous solubility of the title molecule. Another online tool that can be used for prediction of activities based on structure is PASS (Prediction of Activity Spectra) [53]. PASS analysis (Table 6) of the 2-(*p*-(4-phenylbutanecarboxyamido)phenyl)-5-(ethylsulfonyl)benzoxazole predicts amongst other activities, anti-diabetic activity with Pa (Probability to be active) value of 0.430. Diabetes mellitus is characterized by chronic elevated blood glucose levels. Glycogen Phosphorylase (GP), a key enzyme in the regulation of glycogen metabolism, exists in two inter-convertible forms: the dephosphorylated form, GPb, and the phosphorylated form, Gpa. Glycogen phosphorylase a (GPa) has been exploited as a specific target of inhibitors that might prevent glycogenolysis under high glucose conditions in type II diabetes [54,55]. To evaluate the inhibitory nature of the compound against Glycogen Phosphorylase a (Gpa) enzyme, molecular docking studies were carried out. The 3D crystal structure of GPa was obtained from Protein Data Bank (PDB ID: 2GPA) [56]. 2GPA has a good resolution (2 Å) and attached co-crystallized inhibitors were used to identify the active site. Molecular docking is an efficient tool to get an insight into ligand-receptor interactions. All molecular docking calculations were performed on AutoDock-Vina software [57]. The AutoDock Tools (ADT) graphical user interface was used to calculate Kollmann charges for the protein and to add polar hydrogen. Water molecules and co-crystallized ligands were removed. The ligand was prepared for docking by minimizing its energy at M05/6-311 + G(d,p) (5D, 7 F) level of theory. Partial charges were calculated by Geistenger method. Torsion and rotatable bonds were defined. The active site of the enzyme was defined to include residues of the active site within the grid size of 40 Å × 40 Å × 40 Å. Lamarckian Genetic Algorithm (LGA) available in Auto Dock Vina was employed for docking. The docking protocol was tested by removing co-crystallized inhibitor from the protein and then docking it at the same site. To evaluate the quality of docking results, the common way is to calculate the Root Mean Square Deviation (RMSD) between the docked pose and the known crystal structure confirmation. RMSD values up to 2 Å are considered reliable for the docking protocol [58]. The docking protocol we employed predicted a similar confirmation with RMSD value well within the allowed range of 2 Å (Fig. 6). Amongst the docked confirmations of the title compound, the confirmation which was close to the confirmation of co-crystallized ligand and scored well was visualized for ligand-protein interactions in Discover Studio Visualizer 4.0 and pymol software. The ligand binds at the active sites of the protein by weak non-covalent interactions most prominent of which are H-bonding, cation-π and sigma-π interactions. Amino acids viz. Asn284, Phe285, Lys574, Thr676, Gly677 and Arg292 form H-bonds with the ligand (Figs. 7 and 8). The residues Gly135 and Leu136 hold the phenyl rings of the compound by alkyl-π interactions. Glu672 is involved in a cation-π interaction with the ligand. Binding free energy (ΔG in kcal/mol) of −10.7 as predicted by Autodock Vina (Table 7) suggests good binding affinity. The inhibitor forms a stable complex with GPa as is evident from the ligand-receptor interactions.

Table 6
PASS prediction for the activity spectrum of the compound, Pa represents probability to be active and Pi represents probability to be inactive.

Pa	Pi	
0.859	0.002	Muscular dystrophy treatment
0.515	0.059	Gastrin inhibitor
0.409	0.013	Vascular (periferal) disease treatment
0.430	0.036	Antidiabetic
0.392	0.040	Atherosclerosis treatment
0.381	0.034	Alzheimer's disease treatment
0.427	0.083	Antiinflammatory
0.344	0.011	Cyclooxygenase 1 inhibitor
0.399	0.070	5 Hydroxytryptamine release inhibitor
0.403	0.078	Antiarthritic
0.335	0.033	Non-steroidal antiinflammatory agent
0.367	0.067	Hypolipemic
0.299	0.021	Lipoprotein disorders treatment

Table 7
Binding affinity of different poses of the title compound as predicted by Autodock Vina.

Mode	Affinity (Kcal/mol)	Distance from best mode	
		RMSD 1.b.	RMSD u.b.
1	−10.5	0.000	0.000
2	−9.8	2.008	8.346
3	−9.3	2.373	4.794
4	−9.3	2.236	5.186
5	−8.8	2.376	3.548
6	−8.8	12.047	14.496
7	−8.7	4.790	8.273
8	−8.6	2.719	9.762
9	−8.5	3.384	8.217

5. Conclusion

The molecular structural parameters and vibrational wavenumbers have been obtained using density functional theory. Detailed vibrational assignments of the observed IR and Raman bands have been proposed on the basis of potential energy distribution analysis and most of the modes have wavenumbers in the expected range. The molecular electrostatic potential has been mapped for predicting sites and relative reactivity towards electrophilic and nucleophilic attack. The first and second order hyperpolarizabilities are calculated the first order hyperpolarizability is 113.08 times that of the standard NLO material urea and hence the title compound and its derivatives are good objects for future studies of nonlinear optics. In summary,

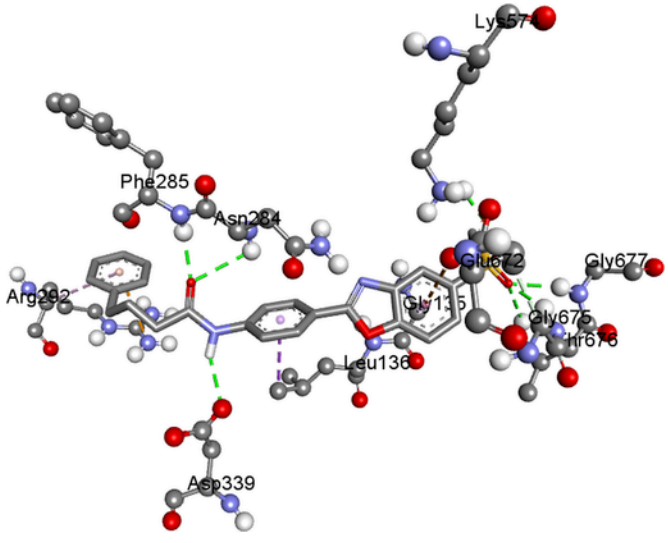

Fig. 6. Ligand-Protein interactions, H-bonds, cation-π and sigma-π interactions are represented by green, orange and violet dotted lines respectively. (For interpretation of the references to colour in this figure legend, the reader is referred to the web version of this article.)

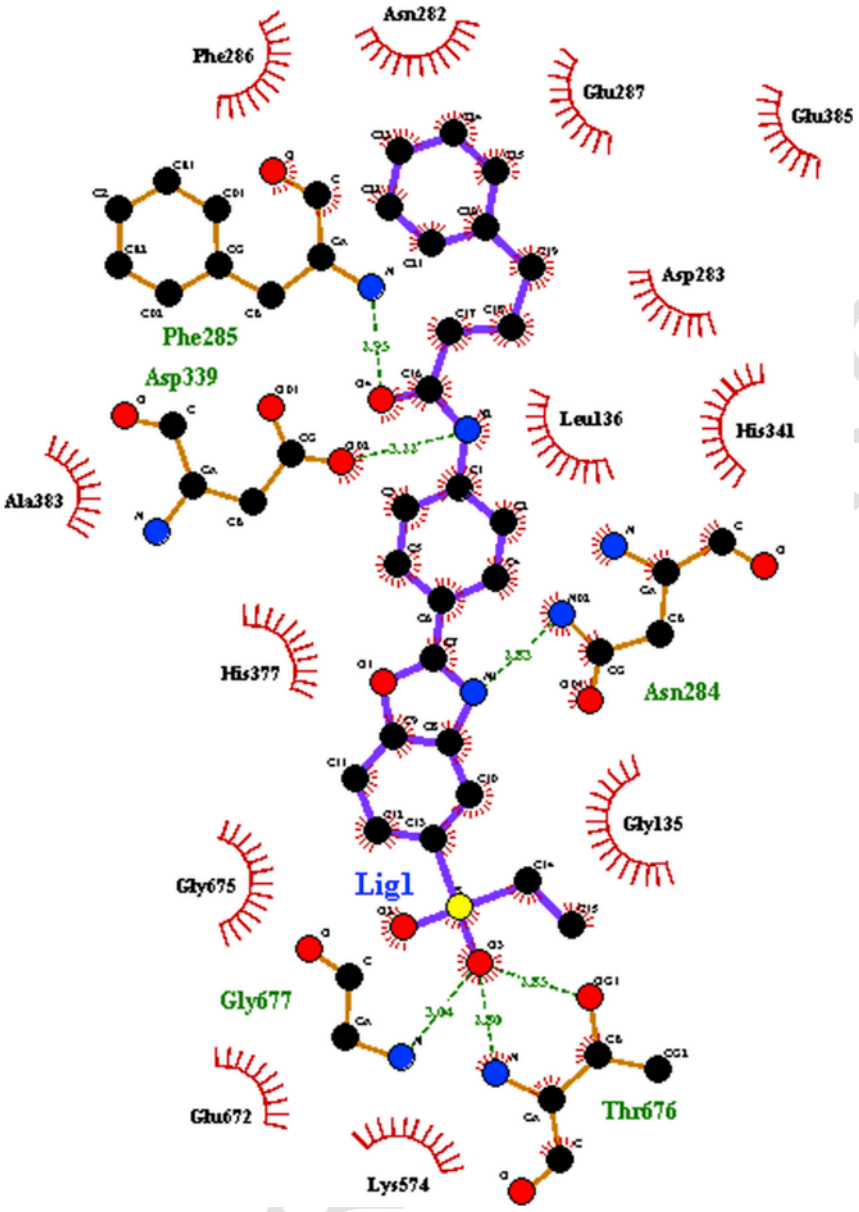

Fig. 7. Ligand-protein interactions, only amino acids are shown, H-bonds are shown by green dotted lines. (For interpretation of the references to colour in this figure legend, the reader is referred to the web version of this article.)

the title compound, 2-[4-(4-phenylbutanamido)phenyl]-5-ethylsulphonyl-benzoxazole was re-synthesized and subjected to pharmacological evaluation. The results showed that it possessed a weak to moderate tyrosinase inhibitory activity and was unsuccessful in inhibition assays against AChE and BChE.

Acknowledgements

The authors would like to extend their sincere appreciation to the Deanship of Scientific Research at King Saud University for funding this work through the Research Group Project No.PRG-1436-23. The authors are thankful to University of Antwerp for access to the University's CalcUA Supercomputer Cluster.

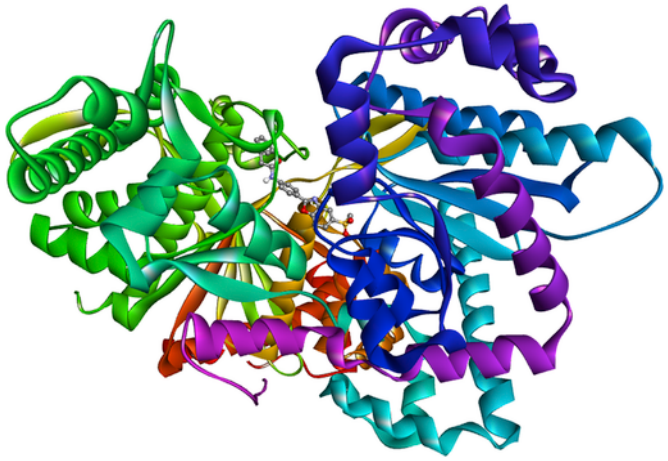

Fig. 8. The ligand and the co-crystallized inhibitor embedded into the catalytic site of GPa.

References

[1] M.J. Don, C.C. Shen, Y.L. Lin, W.J. Syu, Y.H. Ding, C.M. Sun, Nitrogen containing compounds from salvia militorrhiza, J. Nat. Prod. 68 (2005) 1066–1070.

[2] J. Easmon, G. Purstinger, K.S. Thies, G. Heinisch, J. Hofmann, Synthesis, structure activity relationships, and antitumor studies of 2-benzoxazolyl hydrazones derived from alpha-(N)-acyl heteroaromatics, J. Med. Chem. 49 (2006) 6343–6350.

[3] D.C. Tully, H. Liu, P.B. Alper, A.K. Chatterjee, R. Epple, M.J. Roberts, J.A. Williams, K.T. Nguyen, D.H. Woodmansee, C. Tumanut, J. Li, G. Spraggon, J. Chang, T. Tuntland, J.L. Harris, D.S. Karanewsky, Synthesis and evaluation of arylaminoethyl amides as noncovalent inhibitors of cathepsin S. Part 3: Heterocyclic P3, Bioorg. Med. Chem. Lett. 16 (2006) 1975–1980.

[4] G. Yu, S. Yin, Y. Liu, Z. Shuai, D. Zhu, Structures, electronic states and electroluminescent properties of a zinc(II) 2-(2-hydroxyphenyl)benzothiazolate complex, 2003, J. Am. Chem. Soc. 125 (2003) 14816–14824.

[5] I. Yildiz-Oren, I. Yalcin, E. Aki-Sener, N. Ucarturk, Synthesis and structure activity relationships of new antimicrobial active multisubstituted benzazole derivatives, Eur. J. Med. Chem. 39 (2004) 291–298.

[6] I. Yildiz-Oren, B. Tekiner-Gulbas, I. Yalcin, O. Temiz-Arpaci, E. Aki-Sener, N. Altanlar, Synthesis and antimicrobial activity of new 2-[p-substituted-benzyl]-5-[substituted-carbonylamino]benzoxazoles, Arch. Pharm. Weinh. 337 (2004) 402–410.

[7] A. Akbary, I. Oren, O. Temiz-Arpaci, E. Aki-Sener, I. Yalcin, Synthesis and HIV-1 reverse transcriptase inhibitor activity of some 2,5,6-substituted benzoxazole, benzimidazole benzothiazole and oxazolo(4,5-b) pyridine derivatives, Arzneimittelforschung 53 (2003) 266–271.

[8] R.K. Plemper, K.J. Erlandson, A.S. Lakdawala, A. Sun, A. Prussia, J. Boonsombar, E. Aki-Sener, I. Yalcin, I. Yildiz, O. Temiz-Arpaci, B.P. Tekiner, D. Liotta, J.P. Snyder, R.W. Compans, A target site for template based design of measles virus entry inhibitors, Proc. Natl. Acad. Sci. U. S. A. 101 (2004) 5628–5633.

[9] L.L. Liu, X.J. Jia, Y. Zhang, R.S. Wang, X.M. Pan, Theoretical study of 2-phenylbenzoxazole derivatives and derived phenolic Schiff compounds in gas and solution phase, electronic structures and optical properties, J. Mol. Struct. Theochem 960 (2010) 106–114.

[10] M.S. Ober, R.D. Froese, Quinoline-benzoxazole Derived Compounds for Electronic Films and Devices, US 20140183413 A1 Dow Global Technologies Llc, 2014.

[11] A. Enfissi, S. Prigent, P. Colosetti, T. Capiod, The blocking of capacitative calciumentry by 2-aminoethyl diphenylborate (2-APB) and carboxyamidotriazole (CAI) inhibits proliferation in Hep G2 and Huh-7 human hepatoma cells, Cell Calcium 36 (2004) 459–467.

[12] F.G. Perabo, A. Wirger, S. Kamp, H. Lindner, D.H. Schmidt, S.C. Muller, E.C. Kohn, Carboxyamido-triazole (CAI), a signal transduction inhibitor induces growth inhibition and apoptosis in bladder cancer cells by modulation of Bcl-2, Anticancer Res. 24 (2004) 2869–2877.

[13] C.T. Zeyrek, H. Unver, O.T. Arpaci, K. Polat, N.O. Iskeleli, M. Yildiz, Experimental and theoretical characterization of the 2-(4-bromophenyl)-5-ethylsulphonyl-1,3-benzoxazole, J. Mol. Struct. 1081 (2015) 22–37.

[14] O. Temiz-Arpacı, B.E. Cıfcıoglu-Goztepe, F. Kaynak-Onurdag, S. Ozgen, F.S. Senol, I. Erdogan-Orhan, Synthesis and different biological activities of novel benzoxazoles, Acta Biol. Hung. 64 (2013) 249–261.

[15] M.T.H. Khan, Molecular design of tyrosinase inhibitors, a critical review of promising novel inhibitors from synthetic origins, Pure Appl. Chem. 79 (2007) 2277–2295.

[16] G.L. Ellman, K.D. Courtney, V. Andres, R.M. Featherstone, A new and rapid-colorimetric determination of acetylcholinesterase activity, Biochem. Pharmacol. 7 (1961) 88–95.

[17] I. Orhan, S. Aslan, M. Kartal, B. Sener, K.H.C. Baser, Inhibitory effect of Turkish rosamarinus officinalis L. on acetylcholinesterase and butyrylcholinesterase enzymes, Food Chem. 108 (2008) 663–668.

[18] M.J. Frisch, G.W. Trucks, H.B. Schlegel, G.E. Scuseria, M.A. Robb, J.R. Cheeseman, G. Scalmani, V. Barone, B. Mennucci, G.A. Petersson, H. Nakatsuji, M. Caricato, X. Li, H.P. Hratchian, A.F. Izmaylov, J. Bloino, G. Zheng, J.L. Sonnenberg, M. Hada, M. Ehara, K. Toyota, R. Fukuda, J. Hasegawa, M. Ishida, T. Nakajima, Y. Honda, O. Kitao, H. Nakai, T. Vreven, J.A. Montgomery Jr., J.E. Peralta, F. Ogliaro, M. Bearpark, J.J. Heyd, E. Brothers, K.N. Kudin, V.N. Staroverov, T. Keith, R. Kobayashi, J. Normand, K. Raghavachari, A. Rendell, J.C. Burant, S.S. Iyengar, J. Tomasi, M. Cossi, N. Rega, J.M. Millam, M. Klene, J.E. Knox, J.B. Cross, V. Bakken, C. Adamo, J. Jaramillo, R. Gomperts, R.E. Stratmann, O. Yazyev, A.J. Austin, R. Cammi, C. Pomelli, J.W. Ochterski, R.L. Martin, K. Morokuma, V.G. Zakrzewski, G.A. Voth, P. Salvador, J.J. Dannenberg, S. Dapprich, A.D. Daniels, O. Farkas, J.B. Foresman, J.V. Ortiz, J. Cioslowski, D.J. Fox, Gaussian 09, Revision C.01, Gaussian, Inc, Wallingford CT, 2010.

[19] Y. Zhao, D.G. Truhlar, A new local density functional for main-group thermochemistry, transition metal bonding, thermochemical kinetics and noncovalent interactions, J. Chem. Phys. 125 (19) (2006) http://dx.doi.org/10.1063/1.2370993, 194101.

[20] Y. Zhao, N.E. Schults, D.G. Truhlar, Design of density functional by combining the method of constraint satisfaction with parametrization for thermochemistry, thermochemical kinetics, and noncovalent interactions, J. Chem. Theory. Comput. 2 (2) (2006) 364–382.

[21] Y. Zhao, N.E. Schultz, D.G. Truhlar, Exchange correlation functional with broad accuracy for metallic and nonmetallic compounds, kinetics and noncovalent interactions, 161103 J. Chem. Phys. 123 (2005) 13, http://dx.doi.org/10.1063/1.2126975.

[22] J.B. Foresman, in: E. Frisch (Ed.), Exploring Chemistry with Electronic Structure Methods, A Guide to Using Gaussian, Pittsburg, PA, 1996.

[23] R. Dennington, T. Keith, J. Millam, Gaussview, Version 5, Semichem. Inc., Shawnee Missions, KS, 2009.

[24] J.M.L. Martin, C. Van Alsenoy, GAR2PED, a Program to Obtain a Potential Energy Distribution from a Gaussian Archive Record, University of Antwerp, Belgium, 2007.

[25] N.P.G. Roeges, A Guide to the Complete Interpretation of IR Spectra of Organic Compounds, Wiley, New York, 1994.

[26] S.R. Sheeja, N.A. Mangalam, M.R.P. Kurup, Y.S. Mary, K. Raju, H.T. Varghese, C.Y. Panicker, Vibrational spectroscopic studies and computational study of quinoline-2-carbaldehyde benzyol hydrazone, J. Mol. Struct. 973 (2010) 36–46.

[27] G. Varsanyi, Assignments of Vibrational Spectra of Seven Hundred Benzene Derivatives, Wiley, New York, 1974.

[28] N.B. Colthup, L.H. Daly, S.E. Wiberly, Introduction to IR and Raman Spectroscopy, Academic Press, New York, 1990.

[29] C.Y. Panicker, H.T. Varghese, T. Tansani, Spectroscopic studies and Hartree-Fock ab initio calculations of a substituted amide of pyrazine-2-carboxylic acid – C16H18ClN3O, Turk. J. Chem. 33 (2009) 633–646.

[30] J.B. Bhagyasree, J. Samuel, H.T. Varghese, C.Y. Panicker, M. Arisoy, O. Temiz-Arpaci, Synthesis, FT-IR investigation and computational study of 5-[(4-Bromophenyl)acetamido]-2-(4-tert-butylphenyl)benzoxazole, Spectrochim. Acta 115 (2013) 79–91.

[31] R.M. Silverstein, G.C. Bassler, T.C. Morril, Spectrometric Identification of Organic Compounds, 5thedn, John Wiley and Sons Inc., Singapore, 1991.

[32] P.L. Anto, C.Y. Panicker, H.T. Varghese, D. Philip, O. Temiz-Arpaci, B. Tekiner-Gulbas, I. Yildiz, Vibrational Spectroscopic studies and ab initio calculations of 5-methyl-2-(p-fluoro phenyl) benzoxazole, Spectrochim. Acta 67 (2007) 744–749.

[33] A. Rodriguez, M.E. Sanchez-Vergara, V. Garcia-Montalvo, A. Otriz-Rebollo, J.R. Alvarez-Bada, C. Alvarez-Toledano, Electrical and optical properties of copper and nickel molecular materials with tetrabenzo[b,f,n,j][1,5,9,13]tetraazacyclohexadecine thin films grown by the vacuum thermal evaporation technique, Spectrochim. Acta 75 (2010) 479–485.

[34] V.S. Madhvan, H.T. Varghese, S. Mathew, J. Vinsova, C.Y. Panicker, FT-IR, FT-Raman and DFT calculations of 4-Chloro-2-(3,4-dichlorophenyl carbamoyl)phenyl acetate, Spectrochim. Acta 72 (2009) 547–553.

[35] J.B. Bhagyasree, H.T. Varghese, C.Y. Panicker, J. Samuel, C. Van Alsenoy, K. Bolelli, I. Yildiz, E. Aki, Vibrational spectroscopic (FT-IR, FT-Raman, 1H NMR

and UV) investigations and computational study of 5-nitro-2-(4-nitrobenzyl)benzoxazole, Spectrochim, Acta 102 (2013) 99–113.
[36] Y.S. Mary, K. Raju, I. Yildiz, O. Temiz-Arpaci, H.I.S. Nogueira, C.M. Granadeiro, C.Van Alsenoy, FT-IR, FT-Raman, SERS and computational study of 5-ethylsulphonyl-2-(o-chlorobenzyl)benxozazole, Spectrochim. Acta 96 (2012) 617–625.
[37] K. Fukui, Role of frontier orbitals in chemical reactions, Science 218 (1982) 747–754.
[38] R.G. Parr, P.K. Chattaraj, Principle of maximum hardness, J. Am. Chem. Soc. 113 (1991) 1854–1855.
[39] R.J. Parr, L.V. Szentpaly, S. Liu, Electrophilicity index, J. Am. Chem. Soc. 121 (1999) 1922–1924.
[40] R. Parthasarathi, J. Padmanabhan, V. Subramanian, B. Maiti, P. Chattaraj, Toxicity analysis of 33'44'5-pentachloro biphenyl through chemical reactivity and selectivity profiles, Curr. Sci. 86 (2004) 535–542.
[41] Y.R. Shen, The Principles of Nonlinear Optics, Wiley, New York, 1984.
[42] D.M. Burland, R.D. Miller, C.A. Walsh, Second order nonlinearity in poled polymer systems, Chem. Rev. 94 (1994) 31–75.
[43] C. Adant, M. Dupuis, J.L. Bredas, Ab initio study of the nonlinear optical properties of urea, electron correlation and dispersion effects, Int. J. Quantum Chem. 56 (1995) 497–507.
[44] P. Thul, V.P. Gupta, V.J. Ram, P. Tandon, Structural and spectroscopic studies on 2- pyranones, Spectrochim. Acta 75 (2010) 251–260.
[45] P. Politzer, J.S. Murray, Theoretical biochemistry and molecular biophysics, In: D.L. Beveridge, R. Lavery (Eds.), A Comprehensive Survey, Protein, vol. 2, Adenine Press, Schenectady, New York, 1991.
[46] A.D. Becke, Density functional thermochemistry. III. The role of exact exchange, J. Chem. Phys. 98 (1993) 5648–5652.
[47] E.D. Glendening, A.E. Reed, J.E. Carpenter, F. Weinhold, NBO Version 3.1, Gaussian Inc., Pittsburgh, PA, 2003.
[48] I.V. Tetko, J. Gasteiger, R. Todeschini, A. Mauri, D. Livingstone, P. Ertl, V.A. Palyulin, E.V. Radchenko, N.S. Zefirov, A.S. Makarenko, V.Y. Tandchuk, V.V. Prokopenko, Virtual computational chemistry laboratory-design and description, J. Computer-aided Mol. Des. 19 (6) (2005) 453–463.
[49] J. Hadgraft, R. Guy, Selection of drug candidates for transdermal delivery, In: Transdermal Drug Delivery, vol. 1, Marcel Dekker Inc., New York, 1989, pp. pp.60–120.
[50] T. Yano, A. Nakagawa, M. Tsuji, K. Noda, Skin permeability of various non-steroidal anti-inflammatory drugs in man, Life Sci. 39 (12) (1986) 1043–1050.
[51] C. Goosen, J. Du Plessis, D.G. Mullter, L.F.J. Van Rensburg, Correlation between physicochemical characteristics, pharmacokinetic properties and transdermal absorption of NSAID's, Int. J. Pharm. 163 (1) (1998) 203–209.
[52]] Openmolecules.org.2016; available from: http://www.openmolecules.org/properties/properties.html#clogs.
[53] A. Lagunin, A. Stepanchikova, D. Filimonov, V. Poroikov, PASS: prediction of activity spectra for biologically active substances, Bioinformatics 16 (2000) 747–748.
[54] K.A. Watson, E.P. Mitchell, L.N. Johnson, J.C. Son, C.J.F. Bichard, M.G. Orchard, G.W.J. Fleet, N.G. Oikonomakos, D.D. Leonidas, M. Kontou, A.C. Papageorgiou, Design of inhibitors of glycogen phosphorylase, a study of α- and β-C-glucosides and 1-thio-β-D-glucose compounds, Biochemistry 33 (1994) 5745–5758.
[55] N.G. Oikonomakos, M. Kontou, S.E. Zographos, K.A. Watson, L.N. Jhonson, C.J.F. Bichard, G.W.J. Fleet, K.R. Acharya, N-acetyl-betal-D-glucopyranosylamine, a potent T-state inhibitor of glycogen phosphorylase, a comparison with alpha-D-glucose, Protein Sci. 4 (1995) 2469–2477.
[56] N.G. Oikonomakos, K.E. Tsitsanou, S.E. Zographos, V.T. Skamnaki, S. Goldmann, H. Bischoff, Allosteric inhibition of glycogen phosphorylase a by the potential antidiabetic drug 3-isopropyl 4-(2-chlorophenyl)1,4-dihydro-1-ethyl-2-methyl-pyridine-3,5,6-tricarbo xylate, Protein Sci. 8 (1999) 1930–1945.
[57] O. Trott, A.J. Olson, AutoDock Vina: improving the speed and accuracy of docking with a new scoring function, effiecient otimization and multithreading, J. Comput. Chem. 31 (2010) 455–461.
[58] B. Kramer, M. Rarey, T. Lengauer, Evaluation of the FlexX incremental construction algorithm for protein ligand docking, Proteins Struct. Funct. Genet. 37 (1999) 228–241.